Analysis of a Grating Metal Structure With Broad Back-Scattering Field Pattern for Applications in Vehicle Collision Avoidance System

Young-Huang Chou, Shew-Jon Lin, and Shyh-Jong Chung

***Abstract*—In this paper, grating metal structures with broad and flat back-scattering field patterns are studied for possible applications in a vehicle collision avoidance system. The two-dimensional TE scattering of a planar grating structure and a curved grating structure are analyzed at a frequency of 77 GHz. For the planar structure, the method of moment together with Floquet's theorem is used to solve the induced current and the resultant back-scattering field. Based on the results of the planar structure, the scattering field of the curved grating structure is obtained by using a perturbation method. The influence on the field pattern of the curvature as well as other structure parameters, such as the width and geometry of each period in the grating structure, is investigated.**

***Index Terms*—Back-scattering field pattern, collision-avoidance radar, metal grating.**

I. Introduction

INTELLIGENT transportation systems (ITSs) have obtained much attention in both theoretical and practical studies [1], [2]. The systems apply advanced technologies, such as communication, computer, and control, to improve the safety and efficiency of ground transportation, with less congestion, pollution, and environmental impact. Among the various areas of ITS, the vehicle collision avoidance system in automated vehicle control systems (AVCSs) is one that is important and interesting for microwave and millimeter-wave applications. Much work has been devoted to the development of on-vehicle collision avoidance radars (CARs) [3]–[11]. Although radars with operating frequencies of 24, 60, 77, and 94 GHz were developed, those with 77 GHz seem more promising in both Europe and the United States. These radars, which serve as the drivers' electronic eyes, emit frequency-modulated continuous waves or pulsed waves and receive echoes from the environment. Potential hazards from other vehicles or obstacles (such as manmade traffic structures or topographic structures) can thus be sensed and avoided by examining these echoes. However, only at angles near the surface normals of vehicles or obstacles can strong echoes be received. Due to the lack of specular reflections, the received echoes from other angles would be quite weak.

Manuscript received April 20, 2000; revised March 2, 2001 and August 9, 2001. This work was supported in part by the National Science Council, R.O.C., under Grant NSC 89-2213-E-009-050 and in part by the Ministry of Education and the National Science Council, R.O.C., under Contact 89-E-FA06-2-4.

The authors are with the Department of Communication Engineering, National Chiao Tung University, Hsinchu, 300 Taiwan, R.O.C. (e-mail: sjchung@cm.nctu.edu.tw).

Publisher Item Identifier S 0018-9545(02)00444-9.

To solve this problem, it has been suggested in [12] that the planar Van Atta retrodirective antenna array [13], which is formed by several antenna pairs, can be equipped on the vehicles' or obstacles' bodies to enhance the echoes at angles away from normal directions. The Van Atta array possesses the advantage that the reradiated fields from all the transmitting antennas in the array have a coherent phase in the arrival direction of the incident wave, thus yielding a broad back-scattering field pattern. The scattering field level from the array is proportional to the number of the antenna pairs. Thus, to produce a strong radar echo, a large array with many antenna pairs would be needed, making the layout of the transmission lines pairing the antennas complicated.

In this paper, we propose another approach to increase the radar echoes at off-normal directions. Instead of using Van Atta arrays, this approach uses grating metal structures [Fig. 1(a) and (b)] for equipping on vehicles or obstacles to increase the back-scattering field levels. When a radar wave is incident upon the grating structure, surface electric currents with different phases and amplitudes would be induced on all the periods of the metal grating, which, in turn, would radiate electromagnetic field toward the interrogating radar. These induced electric currents may be viewed as an equivalent antenna array. By changing the width and shape of each period in the grating structure, the interelement spacing and the excitation currents of the equivalent array would be changed, and grating lobes may thus appear in and fill up the back-scattering field pattern. The analysis of the grating structures is described in Section II. As a preliminary study and for simplicity, two-dimensional TE scattering problems as shown in Fig. 1(a) and (b) were tackled by using the method of moment [14] together with a perturbation method. Simulation results for the grating structures are presented in Section III. Section IV gives the conclusions.

II. Analysis

A. Planar Grating Structures

Consider the finite periodical metal structure shown in Fig. 1(a), which contains M periods in the x direction $(M \gg 1)$ and is assumed to be infinite in the z direction. A symmetrical triangular structure of width a and height h is located in each period of width b. A TE wave $\bar{E}^i$ of frequency 77 GHz is incident upon the metal structure at an angle of θ. $\bar{E}^i = \hat{z}E^i(x,y) = \hat{z}E_o e^{j(k\sin\theta)x} e^{j(k\cos\theta)y}$. The total width W $(=\text{Mb})$ of the whole structure is assumed to be far larger than the wavelength λ $(=3.9\ \text{mm})$ of the incident field.

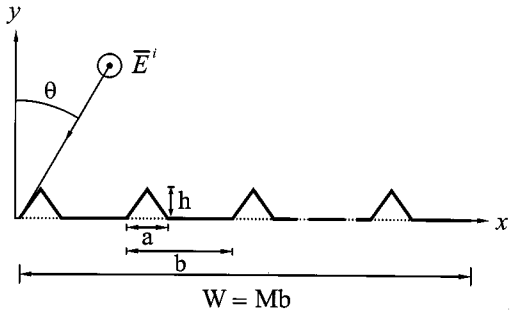

(a)

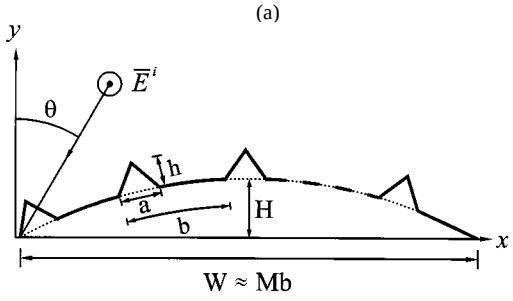

(b)

Fig. 1. (a) A planar grating metal structure and (b) a curved grating metal structure.

To calculate the back-scattering field, the induced surface current on the metal structure should be solved. Since there are many periods in the structure, the induced current on each period can be assumed to be the same as that of a structure with infinite periods. According to Floquet's theorem [15], the induced currents on all the periods of an infinitely periodical structure are the same except for a phase difference of $kb\sin\theta$ between adjacent currents. This phase difference comes from the phase difference of the incident field at different periods. Therefore, only the current distribution $\bar{J}_0(x,y)$ $(=\hat{z}J_0(x,y))$ in a period needs to be solved. By using the mixed potential formulation [16], the total scattering field $\bar{E}^s$ $(=\hat{z}E^s(x,y))$ from the infinitely periodical structure can be expressed as

$$E^s(x,y) = -j\omega\mu \int_C J_0(x',y') G_{\rm prd}(x,y;x',y')\, dl' \qquad (1)$$

in which the relationship $\nabla \cdot \hat{J}_0 = 0$ has been incorporated. "C" denotes the contour along the surface of a period. $G_{\rm prd}(x,y;x',y')$ is the Green's function of the infinitely periodic structure, which can be derived as [17]

$$G_{\rm prd}(x,y;x',y') = \frac{1}{b}\sum_{p=-\infty}^{\infty} \frac{e^{-j\beta_y|y-y'|}}{2j\beta_y} e^{j\beta_{xp}(x-x')} \qquad (2)$$

with

$$\beta_{xp} = \frac{2\pi p}{b} + k\sin\theta, \quad \beta_y = \sqrt{k^2-\beta_{xp}^2}. \qquad (3)$$

Applying the boundary condition on the metal, that is, $\bar{E}^i + \bar{E}^s = 0$, an integral equation for the unknown current J_0 is obtained

$$E_o e^{j(k\sin\theta)x} e^{j(k\cos\theta)y} = j\omega\mu \int_C J_0(x',y') \times G_{\rm prd}(x,y;x',y')\, dl', \quad (x,y)\in C. \qquad (4)$$

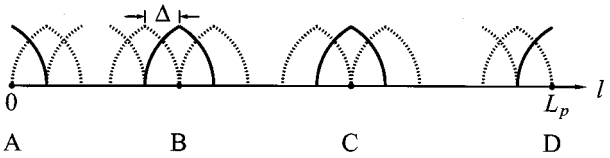

Fig. 2. Basis functions for the induced current in a period of the grating structure. "A," "B," and "C" are the tip points of the triangle in the period and "D" is the end point of the period. The solid curves represent the basis functions for these breaking points, and the dotted curves are those for other sampling points.

To solve (4) using the method of moment, the current J_0 is expanded by piecewise sinusoidal basis functions as shown in Fig. 2

$$J_0(l) = \sum_{n=1}^{N} a_n u_n(l), \quad 0 < l < L_p \qquad (5)$$

where L_p $(=2\sqrt{h^2+a^2/4}+b-a)$ is the total length along C, N is the number of basis functions, and u_n is the nth basis

$$u_n(l) = \begin{cases} \dfrac{\sin k(\Delta - |l-l_n|)}{\sin k\Delta}, & l_{n-1} < l < l_{n+1} \\ 0, & \text{otherwise} \end{cases} \qquad (6)$$

with $\Delta = L_p/(N-1)$ and $l_n = (n-1)\Delta$, for $n > 0, l_{-1} = l_0 = 0$.

By casting (5) into (4) and using Galerkin's procedure, an $N \times N$ matrix equation is obtained from which the unknown expansion coefficients a_n and thus the current distribution J_0 can be solved. It is noticed that from Floquet's theorem, a_N $(=J_0(L_p))$ should be equal to $a_1 e^{jkb\sin\theta}$ $(=J_0(0)e^{jkb\sin\theta})$. This constraint must be applied when solving the matrix equation. Finally, by remembering that the current of any period is the same as J_0 except a phase difference of a multiple of $kb\sin\theta$, the total induced current $J(x,y)$ on the finite periodic structure of Fig. 1(a) can be approximated as

$$J(x,y) = \sum_{m=0}^{M-1} J_0(x-mb,y) e^{jmkb\sin\theta}. \qquad (7)$$

The back-scattering field $E^{\rm bs}$ at a far point $(x,y) = (r\sin\theta, r\cos\theta)$, with $r = \sqrt{x^2+y^2} \gg W$, can be calculated by using (1) with $J_0(x',y')$ replaced by the total current $J(x',y')$ and $G_{\rm prd}(x,y;x',y')$ replaced by the asymptotic Green's function of a z-directed line source $G(r,\theta;x',y')$

$$G(r,\theta;x',y') = \frac{1}{4j}\sqrt{\frac{2j}{\pi k}}\frac{e^{-jkr}}{\sqrt{r}} e^{jk(\sin\theta x' + \cos\theta y')}. \qquad (8)$$

The result turns out to be

$$E^{\rm bs}(r,\theta) = E_0^{\rm bs}(r,\theta)\sum_{m=0}^{M-1} e^{2jmkb\sin\theta} = E_0^{\rm bs}(r,\theta)\left(\frac{1-e^{2jMkb\sin\theta}}{1-e^{2jkb\sin\theta}}\right) \qquad (9)$$

where $E_0^{\rm bs}(r,\theta)$ is the radiation field due to the induced current J_0 of a single period

$$E_0^{\rm bs}(r,\theta) = -\frac{\omega\mu}{4}\sqrt{\frac{2j}{\pi k}}\frac{e^{-jkr}}{\sqrt{r}}\int_C J_0(x',y') \times e^{jk(\sin\theta x' + \cos\theta y')}\, dl'. \qquad (10)$$

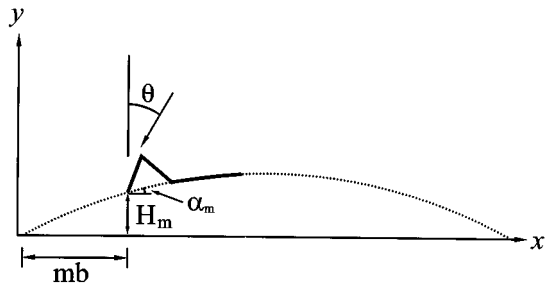

Fig. 3. The mth period of the curved grating structure.

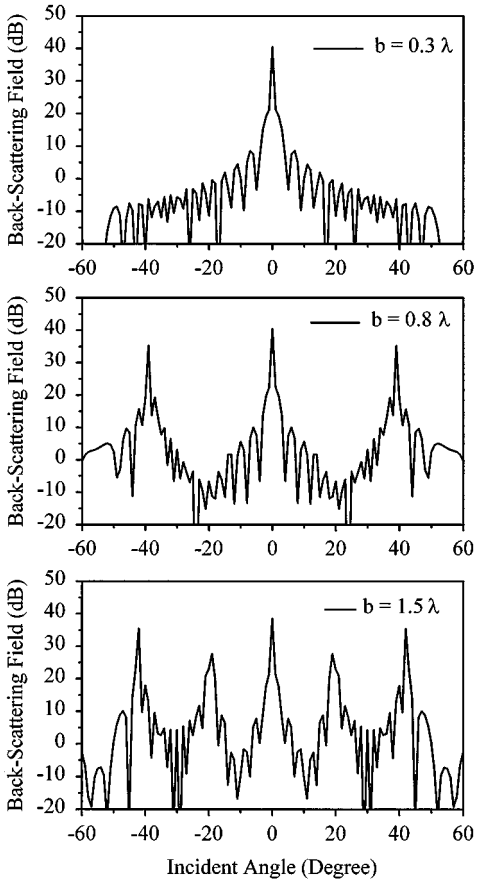

Fig. 4. Back-scattering field patterns of planar triangular grating structure with $b = 0.3\lambda, 0.8\lambda$, and 1.5λ. $W = 20$ cm, $h = 3$ mm, $a = b$, $f = 77$ GHz.

It is seen from (9) that due to the round-trip phase difference, the back-scattering field from the mth period is equal to $E_0^{\rm bs}(r,\theta)$ plus a phase excess of $2kmb\sin\theta$. Also, similar to an antenna array, the total back-scattering field pattern of the finite periodic structure equals the product of an element pattern $E_0^{\rm bs}(r,\theta)$ and an array factor $(1-e^{2jMkb\sin\theta})/(1-e^{2jkb\sin\theta})$.

B. Curved Grating Structures

The curved grating structure shown in Fig. 1(b) is formed by periodically putting M triangular metal structures on a metal arc surface of width W and height H. The arc height H is assumed much smaller than the arc width W, so that the curved grating structure may be considered as a perturbation of the planar grating one. The distribution of the induced current amplitude on each period is thus assumed to be the same as that of the planar structure, i.e., $|J_0(x,y)|$. The current phase is modified by incorporating the phase deviation of the incident field at the structure surface due to the perturbation of the structure. Consider the mth period of the grating structure, which is located at a height H_m above the x–z plane and with a tilt angle of α_m (Fig. 3). For a point (x,y) on the period's surface, an approximate height deviation of $H_m + (x - mb)\tan\alpha_m$ is introduced due to the structure perturbation. The incident field arriving at that point would thus have a small extra phase excess of $k(H_m+(x-mb)\tan\alpha_m)\cos\theta$. Therefore, the induced current $J_m(x,y)$ on the mth period is approximated as

$$J_m(x,y) = J_0(x-mb,y)e^{jmkb\sin\theta} \times e^{jk(H_m+(x-mb)\tan\alpha_m)\cos\theta} \tag{11}$$

which corresponds to a back-scattering field of

$$E_m^{\rm bs}(r,\theta) = -\frac{\omega\mu}{4}\sqrt{\frac{2j}{\pi k}}\frac{e^{-jkr}}{\sqrt{r}}e^{2jmkb\sin\theta} \cdot \int_C J_0(x',y')e^{jk(\sin\theta x'+\cos\theta y')} \times e^{2jk(H_m+x'\tan\alpha_m)\cos\theta}\,dl'. \tag{12}$$

Note that the integration is along the contour C, which is the surface of a period of the unperturbed (planar) structure. The total back-scattering field $E^{\rm bs}$ of the curved grating structure is obtained by summing the contributions from all the periods, i.e.,

$$E^{\rm bs}(r,\theta) = \sum_{m=0}^{M-1} E_m^{\rm bs}(r,\theta). \tag{13}$$

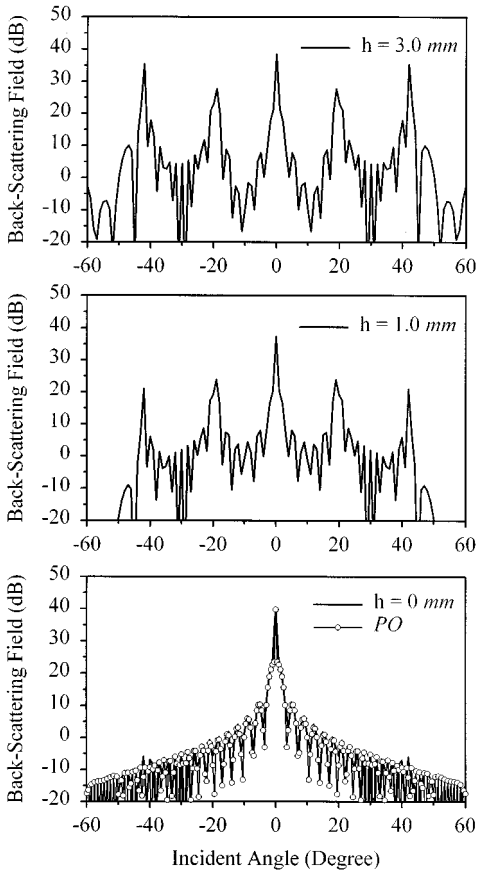

Fig. 5. Back-scattering field patterns of planar triangular grating structure with $h = 3$ mm, 1 mm, and 0 mm. $W = 20$ cm, $b = a = 1.5\lambda$, $f = 77$ GHz. The result of $h = 0$ mm calculated by the PO method is shown in the bottom figure for comparison.

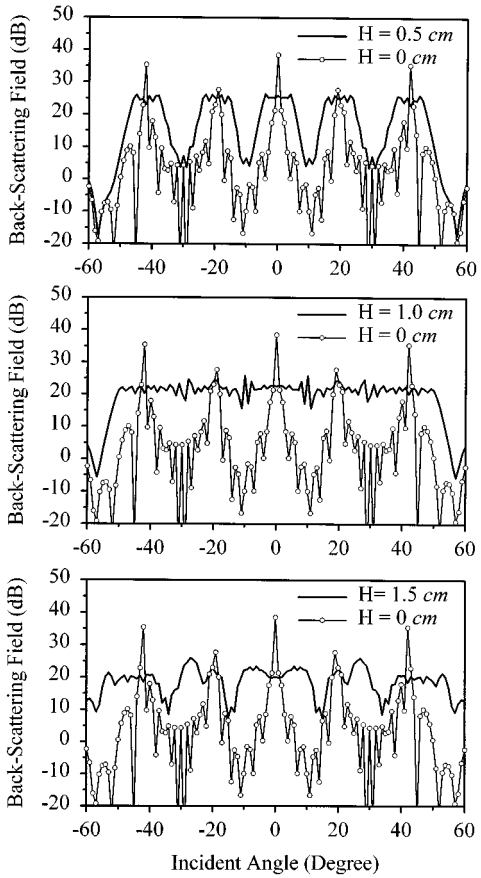

Fig. 6. Back-scattering field patterns of the curved triangular grating structure with $H = 0.5$, 1.0, and 1.5 cm. $W = 20$ cm, $b = a = 1.5\lambda$, $h = 3$ mm, $f = 77$ GHz. The results of the planar grating structure ($H = 0$) are shown for comparison.

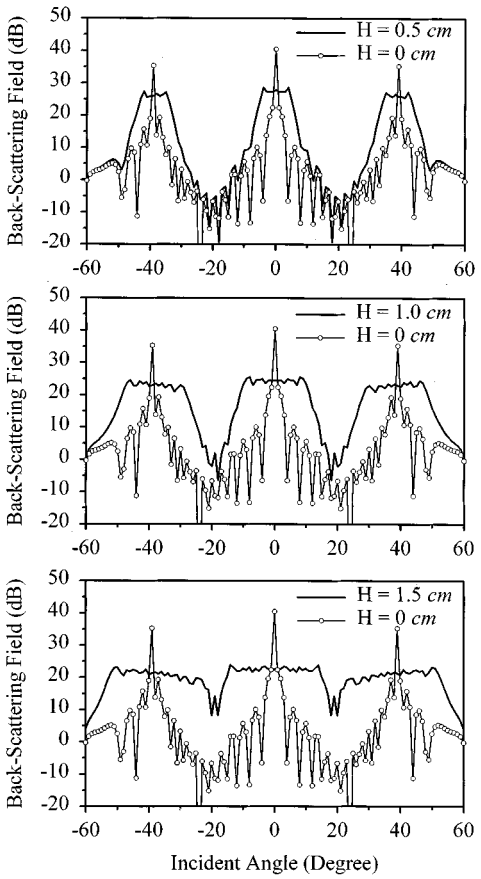

Fig. 7. Back-scattering field patterns of the curved triangular grating structure with $H = 0.5$, 1.0, and 1.5 cm. $W = 20$ cm, $b = a = 1.5\lambda$, $h = 3$ mm, $f = 77$ GHz. The results of the planar grating structure ($H = 0$) are shown for comparison.

III. Simulation Results

After the analysis, a method-of-moment code has been finished to simulate the back-scattering effects of the grating structures. The widths of the grating structures are set to be 20 cm, i.e., $W = 20\,\text{cm} \approx 51\lambda$. Fig. 4 compares the back-scattering field patterns of planar grating structures with period widths b equal to 0.3λ, 0.8λ, and 1.5λ. The triangular grating's width a is the same as the period width b, and the grating's height h equals 3 mm. As is seen, the field pattern for $b = 0.3\lambda$ has only one main lobe, while those for $b = 0.8\lambda$ and 1.5λ have more than one. The wider the period is, the higher the number of field lobes and the closer is the spacing between lobes. When examining (9), it is found that the number and spacing of the main lobes are determined by the "array factor," which in turn is controlled by the period width b. As b is larger than 0.5λ, multiple main lobes would appear in the range of visible angles. For the planar grating structure of $b = 1.5\lambda$, Fig. 5 shows the influence of the grating's height h on the back-scattering field pattern. The main lobe number stays the same when h is reduced from 3 to 1 mm, but the lobe levels and lobe beamwidths are reduced for the side main lobes. As h is further reduced to zero, the grating structure becomes a flat metal strip, and the side main lobes completely vanish. As a numerical check, the simulation result using the physical optics (PO) method for the flat strip is also shown. It is seen that the results calculated by the two different methods agree quite well.

Although increasing the period width may increase the main lobe number, the back-scattering field still changes violently with the change of the incidence angle. Only at the angles where the main lobes are located can strong back-scattering fields be received. To release this limitation, one may arch the grating structure to increase the beamwidths of the main lobes. Fig. 6 shows the back-scattering field patterns of the curved grating structures with arc heights H of 0.5, 1.0, and 1.5 cm. The period width b equals 1.5λ and the grating's height h equals 3 mm. The field pattern of the planar grating structure, i.e., the curved grating structure with $H = 0$, is also shown for comparison. For the planar grating structure with $b = 1.5\lambda$, there are five sharp main lobes in the range $-60^\circ < \theta < 60^\circ$. As the structure is arched with height of 0.5 cm, the five main lobes become broader, at the expense of reduced lobe levels. When H is further increased to 1.0 cm, as shown in the middle figure, the lobes' beamwidths are wide enough so that the five lobes become connected to each other. At this condition, the whole back-scattering field pattern of the grating structure is quite flat in the range of $-50^\circ < \theta < 50^\circ$. A broad back-scattering beam as wide as 100° is obtained. Further arching the structure to $H = 1.5$ cm would over-broaden the main lobes and cause interference between lobes, thus producing a fluctuating field pattern as shown in the bottom. As another example, Fig. 7 illustrates the influence of the arc height H on the field pattern of the grating structure with period width $b = 0.8\lambda$. Since the

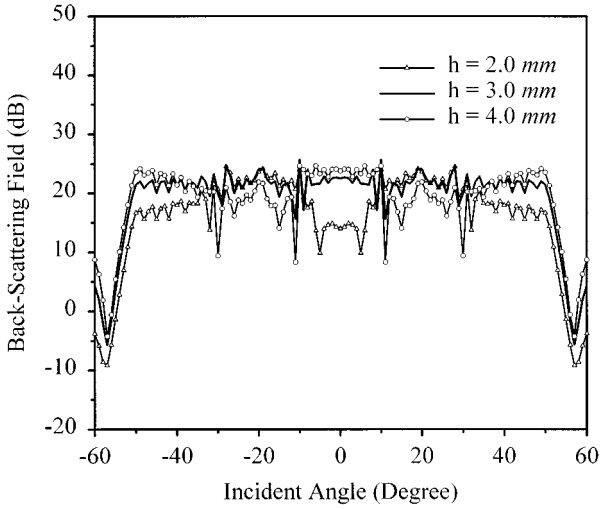

Fig. 8. Back-scattering field patterns of the curved triangular grating structure for different grating height h. $W = 20$ cm, $H = 1.0$ cm, $b = a = 1.5\lambda$, $f = 77$ GHz.

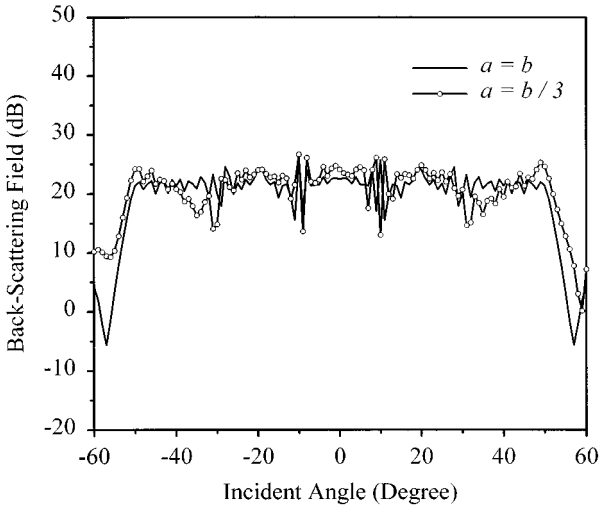

Fig. 9. Back-scattering field patterns of the curved triangular grating structure with $a = b/3$ and $a = b$. $W = 20$ cm, $H = 1.0$ cm, $b = 1.5\lambda, h = 3$ mm, $f = 77$ GHz.

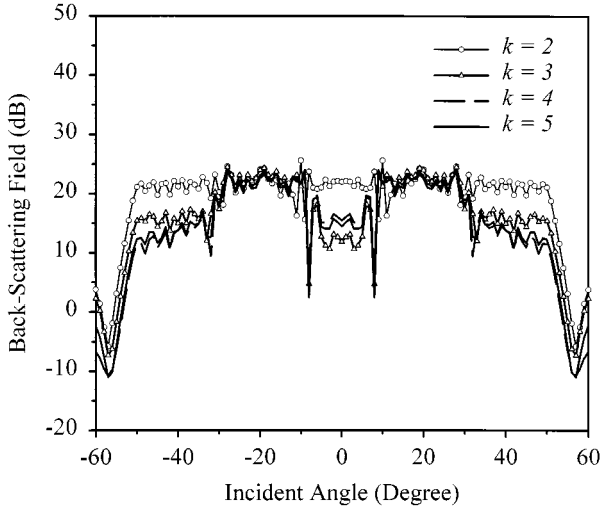

Fig. 10. Back-scattering field patterns of curved multangular grating structures. $W = 20$ cm, $H = 1.0$ cm, $b = a = 1.5\lambda, h = 3$ mm, $f = 77$ GHz.

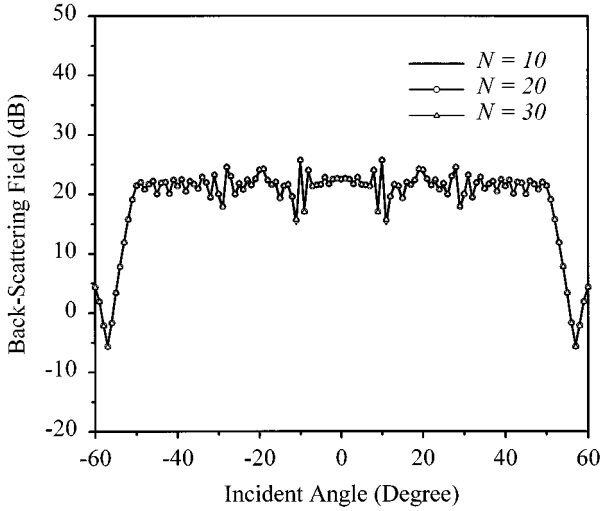

Fig. 11. Back-scattering field patterns calculated by using different number (N) of basis functions. $W = 20$ cm, $H = 1.0$ cm, $b = a = 1.5\lambda, h = 3$ mm, $f = 77$ GHz.

main-lobe spacing of the corresponding planar grating structure is increased as compared to that of $b = 1.5\lambda$, a larger arc height is needed to broaden the main-lobe beamwidths so that a flat back-scattering field pattern may be achieved. As shown in the figure, the required arc height would be larger than 1.5 cm.

For the curved grating structure of $H = 1.0$ cm and $b = a = 1.5\lambda$, Fig. 8 shows the field patterns for a grating height $h = 2$, 3, and 3.5 mm. The field pattern is approximately the same when the grating's height is increased from 3 to 3.5 mm. But when h is reduced to 2 mm, the field pattern is a little deteriorated and has about 10 dB down in the range of $|\theta| < 8°$.

Next, the effects of the geometry of the grating structure are to be studied. Fig. 9 compares the back-scattering field pattern for the curved grating structure of $a = b/3$ to that of $a = b$. The other structure parameters are fixed as $H = 1.0$ cm, $b = 1.5\lambda$, and $h = 3$ mm. As can be seen, although the triangles' width a is reduced to one-third of the original one, the field pattern of $a = b/3$ has little change as compared to that of $a = b$, which means that the triangles' width is a minor factor in the design of the grating structure. As compared to the result of the triangular grating, Fig. 10 shows the field patterns of several multangular gratings. $H = 1.0$ cm and $b = 1.5\lambda$. The metal surface in each period is piecewise-linear and with k equal segments. The end points of the segments are located on an arc of width $a = b$ and height $h = 3$ mm. As shown in the figure, the field levels at $|\theta| < 8°$ and $30° < |\theta| < 50°$ for the structures of $k > 2$ are lower than those of the triangular grating structure $(k = 2)$. Also, the field pattern becomes convergent when the segment number k increases. (Note that as k approaches infinity, the piecewise-linear metal surface in each period becomes an arc surface.)

As a numerical check, Fig. 11 depicts the field patterns of curved triangular grating structures calculated by using a different number (N) of basis functions in expanding the induced current of a period. $H = 1.0$ cm, $b = a = 1.5\lambda$, and $h = 3$ mm. As seen in the figure, no obvious difference is distinguished over

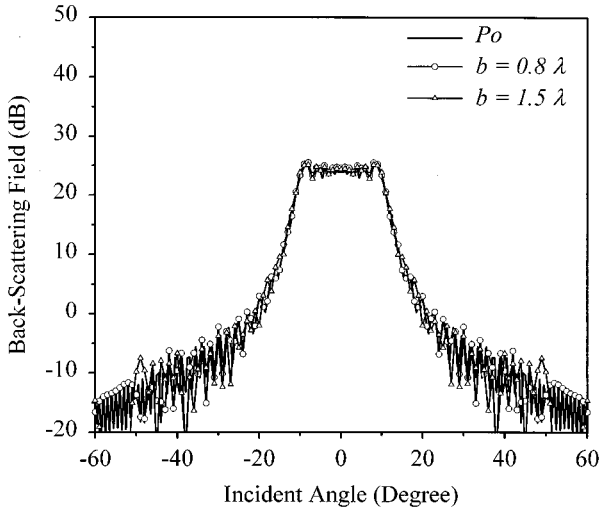

Fig. 12. Back-scattering field patterns calculated by using the PO method and the method of moment with $b\ (=a) = 0.8\lambda$ and 1.5λ. $W = 20$ cm, $H = 1.0$ cm, $h = 0$ mm, $f = 77$ GHz.

the entire range of incident angles, which implies the convergence of the numerical work. As another check, the field patterns of the curve structure with arc height H equal to 1.0 cm but without grating ($h = 0$ mm) are calculated by using the present method (with $b = 0.8\lambda$ and 1.5λ) and the PO method. The results are shown in Fig. 12. Since no grating exists in the structure, there is only one main lobe in the field pattern. Due to the arching of the structure, the beamwidth of this lobe is broad as compared to that of the flat strip of the same width (bottom figure of Fig. 5). As can be seen, the field patterns calculated by the present method match well and agree with that by the PO method.

IV. Conclusion

In this paper, two-dimensional grating metal structures with broad back-scattering field patterns have been studied by using the method of moment together with a perturbation method. The curvature of the grating structure and the width and shape of each period were changed to examine their influences on the field patterns. The validity of the numerical work has been checked by using the convergence test and by comparing the results to those of the PO method. It has been found that arching the grating structure is necessary to produce a broad and flat back-scattering field pattern. The required arc height is dependent on the period width of the grating structure. A smaller period width should be accompanied with a larger arc height. As compared to the large influence of the structure curvature and period width, the geometry of each period has a minor effect on the field pattern.

References

[1] B. Mcqueen and J. Mcqueen, *Intelligent Transportation Systems Architectures*. Boston, MA: Artech House, 1999.
[2] Y. Zhao, *Vehicle Location and Navigation Systems*. Boston, MA: Artech House, 1997.
[3] H. P. Groll and J. Detlefsen, "History of automotive anticollision radars and final experimental results of a mm-wave car radar developed on the Technical University of Munich," in *Proc. 1996 CIE Int. Conf. Radar*, 1996, pp. 13–17.
[4] H. H. Meinel, "Automotive radar and related traffic applications of millimeterwaves," in *1997 Topical Symp. Millimeter Waves*, 1998, pp. 151–154.
[5] B. G. Porter and S. S. Gearhart, "77 GHz dual polarized slot-coupled patches on Duroid with Teflon lenses for automotive radar systems," in *1998 IEEE AP-S Int. Symp.*, vol. 1, 1998, pp. 332–335.
[6] H. H. Meinel, "Commercial applications of millimeterwaves: History, present status, and future trends," *IEEE Trans. Microwave Theory Tech.*, vol. 43, pp. 1639–1653, July 1995.
[7] M. E. Russell, A. Crain, A. Curran, R. A. Campbell, C. A. Drubin, and W. F. Miccioli, "Millimeter-wave radar sensor for automotive intelligent cruise control (ICC)," *IEEE Trans. Microwave Theory Tech.*, vol. 45, pp. 2444–2453, Dec. 1997.
[8] Y. Campos-Roca, L. Verweyen, M. Neumann, M. Fernandez-Barciela, M. C. Curras-Francos, E. Sanchez-Sanchez, A. Hulsmann, and M. Schlechtweg, "Coplanar pHEMT MMIC frequency multipliers for 76-GHz automotive radar," *IEEE Microwave Guided Wave Lett.*, vol. 9, pp. 242–244, June 1999.
[9] K. W. Chang, H. Wang, G. Shreve, J. G. Harrison, M. Core, A. Paxton, M. Yu, C. H. Chen, and G. S. Dow, "Forward-looking automotive radar using a W-band single-chip transceiver," *IEEE Trans. Microwave Theory Tech.*, vol. 43, pp. 1659–1668, July 1995.
[10] P. L. Lowbridge, "Low cost millimeter-wave radar systems for intelligent vehicle cruise control applications," *Microwave J.*, vol. 38, pp. 20–33, Oct. 1995.
[11] T. Yoneyama, "Millimeter-wave research activities in Japan," *IEEE Trans. Microwave Theory Tech.*, vol. 46, pp. 727–733, June 1998.
[12] S.-J. Chung and K. Chang, "A retrodirective microstrip antenna array," *IEEE Trans. Antennas Propagat.*, vol. 46, pp. 1802–1809, Dec. 1998.
[13] L. C. Van Atta, "Electromagnetic Reflector,", Oct. 1959.
[14] R. F. Harrington, *Field Computation by Moment Methods*. Malabar, FL: Krieger, 1983.
[15] R. E. Collin, *Field Theory of Guided Waves*, 2nd ed. New York: IEEE, 1991.
[16] T. Itoh, Ed., *Numerical Techniques for Microwave and Millimeter-Wave Passive Structures*. New York: Wiley, 1989, ch. 3.
[17] R. E. Jorgenson and R. Mittra, "Efficient calculation of the free-space periodic Green's function," *IEEE Trans. Antennas Propagat.*, vol. 38, pp. 633–642, May 1990.

Young-Huang Chou was born in I-Lan, Taiwan, R.O.C. He received the B.S. degree from Ta Tung University, Taipei, Taiwan, in 1992 and the M.S. and Ph.D. degrees from National Chiao Tung University, Hsinchu, Taiwan, in 1994 and 2001, respectively.

His research interests include designs and applications of active and passive integrated antennas, integrated multilayer ceramic circuits, and propagation of transmission lines.

Shew-Jon Lin, photograph and biography not available at the time of publication.

Shyh-Jong Chung was born in Taipei, Taiwan, R.O.C. He received the B.S.E.E. and Ph.D. degrees from National Taiwan University, Taipei, in 1984 and 1988, respectively.

Since 1988, he has been with the Department of Communication Engineering, National Chiao Tung University, Hsinchu, Taiwan, where he is currently a Professor. From 1989 to 1991, he served in the Taiwan Army as a Second Lieutenant, where he was in charge of the maintenance of communication equipment. From September 1995 to August 1996, he was a Visiting Scholar in the Department of Electrical Engineering, Texas A&M University, College Station. His areas of interest include the designs and applications of active or passive planar antennas, communications in intelligent transportation systems, propagation and scattering of transmission lines, packaging effects of microwave circuits, and numerical techniques in electromagnetics.